Received: 16 August 2018 | Revised: 29 November 2018 | Accepted: 12 December 2018

DOI: 10.4218/etrij.2018-0454

SPECIAL ISSUE

WILEY ETRI Journal

Computational load reduction by avoiding the recalculation of angular redundancy in computer-generated holograms

Jia Jia | **Jhensi Chen** | **Daping Chu**

Center for Photonic Devices and Sensors, University of Cambridge, Cambridge, UK.

Correspondence
Daping Chu, Center for Photonic Devices and Sensors, University of Cambridge, Cambridge, UK.
Email: dpc31@cam.ac.uk

A fast hologram calculation approach is proposed to reduce computational load by avoiding the recalculation of redundancy information. In the proposed method, the hologram is divided into several sub-holograms that record and reconstruct different views of 3D objects. The sub-hologram is generated from its adjacent calculated sub-holograms by only adding the holograms of difference images between an adjacent pair of views. The repetitive information of two adjacent views is called angular redundancy. Therefore, avoiding the recalculation of this angular redundancy can considerably reduce the computational load. Experimental results confirm that the proposed method can reduce the computational time for the statue head, rabbits, and car to 4.73%, 6.67%, and 10.4%, respectively, for uniform intensity, and to 56.34%, 57.9%, and 66.24%, respectively, for 256 levels intensity, when compared to conventional methods.

KEYWORDS
computer holography, holographic display, holography

1 | INTRODUCTION

Holographic displays can reconstruct the whole wave-front of 3D objects. Therefore, it can produce all depth cues that the human eye needs, which is regarded as a promising approach for true 3D displays. In holographic displays, the computer-generated hologram (CGH) is calculated and used to reconstruct 3D images. There are many different methods to generate the CGHs of 3D objects. Among them, coherent ray trace (CRT) method is a simple and widely used technique which can achieve a 3D image with higher quality, but at the cost of a heavy computational load, which can be defined by the calculated number of object points to the holograms. To reduce the computation load of the CRT method, various approaches were proposed [1–6]. However, only a few studies focused on reducing redundant information, which implies the information that was repetitive or not perceived by human eyes. We categorized this redundant information into frequency, spatial axis, and temporal redundancy factors based on previous studies.

Initially, a non-uniform sampling method by reducing redundant frequency samples [7] was introduced. In traditional computer hologram calculation methods, the sampling frequency of a CGH is consistent across the whole region and it is twice the maximum frequency of the fringe pattern based on the Shannon–Nyquist sampling theorem. However, the hologram of a single light point is a few concentric rings which are denser from the center towards the periphery; subsequently, this suggests different segments of the hologram have different frequencies. Based on this factor, the non-uniform sampling method reduces the computational load by reducing the frequency sampling number of the CGH.

Considering the spatial axis redundancy, the compressed looked-up table (C-LUT) method [8,9] defines three spatial light modulation factors to calculate the holograms according to the three modulation directions in 3D space and

reduces the repetitive calculation of these factors. In C-LUT, the object points with the same depth have the same longitudinal light modulation factor, and these points have the same distribution in the horizontal direction or in the vertical direction; consequently, they share the same horizontal or vertical light modulation factors. Therefore, there are repetitive calculations for spatial light modulation factors. This type of repetitive calculation is defined as spatial axis redundancy. After reducing this spatial axis redundancy, the calculation load was largely reduced.

In 3D video hologram generation, a large number of temporal sampling is necessary to achieve continuous dynamic frame rate. As neighboring moving frames differ slightly from each other, they may contain stationary areas that will not change between the consecutive video frames. This results in a high similarity between their holograms. This similarity between neighboring video frames suggests that there is a calculation redundancy, which is defined as temporal redundancy and can be removed [1,10].

Besides frequency, spatial axis, and temporal redundant information, hologram calculation may involve angular redundancy, which we define as the repeated or undetected information from adjacent views. Theoretically, there is very limited angular redundancy of real 3D objects, considering the intensity and depth change owing to the different viewing points. However, the limitations of human eyes introduce much more angular redundancy; moreover, the amount of angular redundancy can be increased by the quantification of the angular intensity and depth of 3D objects. For example, each sample point of the hologram records and reconstructs different views of 3D objects. When the density of sampling viewpoints per unit of angle is high, the content changes owing to the miniscule parallax between adjacent viewing points, which cannot be distinguished by human eyes. In other words, most parts of images from adjacent views are the same, and their holograms are similar. This implies there are repeated computations to remove. Based on this idea, a fast hologram calculation method was proposed. The hologram was divided into different segments related to different angular viewpoints, and the angular redundancy of each neighboring segment was identified. The results demonstrated a considerable reduction in computational load by avoiding recalculation of this angular redundancy.

2 | PROPOSED COMPUTATIONAL LOAD REDUCTION METHOD

2.1 | Angular redundant information identification

The principle of the proposed method is shown in Figure 1. It was assumed that the 3D scene will be reconstructed by

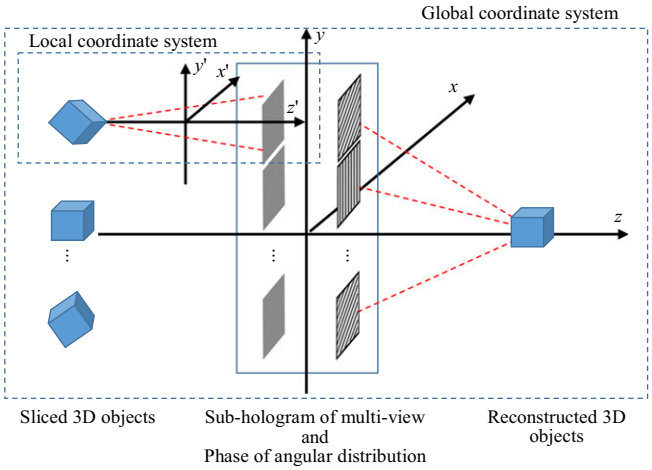

FIGURE 1 Principle of the proposed method

several sliced 2D images, and each sliced 2D image is composed of point sources projected on the plane from its 3D points cloud. The hologram was divided into several sub-holograms, each of which recorded one view of the 3D scene and maintained its own local coordinate system. The occlusion culling method [11] was used to obtain the angular sampling points of the 3D scene with hidden parts removal. The sub-hologram H_{sub} was calculated by (1):

$$H_{\text{sub}} = \sum_{j=1}^{M} A_j \exp\left(i\frac{2\pi}{\lambda} r_j\right), \tag{1}$$

where

$$r_j = \sqrt{(x' - x'_j)^2 + (y' - y'_j)^2 + (d - z'_j)^2} \tag{2}$$

is the distance between the object point $O_n(x'_j, y'_j, z'_j)$ on the 3D object and the $(x', y', 0)$ pixel on the sub-hologram H_{sub}; M is the number of object points; d is the distance between the objects and the hologram plane; A_j is the wave amplitude of the sampling object points; λ is the wavelength.

The phase φ_{sub} was added into each sub-hologram H_{sub} to direct the light into the given direction. Then, all the sub-holograms were tiled up to form the final hologram. The phase φ_{sub} was calculated by (3):

$$\phi_{\text{sub}} = \frac{2\pi}{\lambda}(x' \sin\theta_x + y' \sin\theta_y), \tag{3}$$

where θ_x and θ_y are the angular sampling distances of each view in x and y directions, respectively, in the global coordinate system.

Here, we present a more detailed explanation of the angular redundant information. Initially, the common object points of two adjacent views were defined as the object points with identical intensity and coordinate values. It is noted that the common object points do not necessarily represent the points at the same global location but can be different object points with the same intensity

and the same local coordinate value, as shown in Figure 2A. O_1 and O_2 are two different object points. As their intensity and local coordinate value were the same, they were written as $O_1(x'_j, y'_j, z'_j) = O_2(x'_j, y'_j, z'_j)$, their holograms were also the same. Because the hologram of the common object points only needs to be calculated once, it saves a lot of computational load. This method of avoiding repetitive computation of common object points between a pair of adjacent views is called angular redundancy cutting. Based on this idea, the flowchart for calculating the hologram is shown in Figure 2B.

For the implementation procedure, the hologram corresponding to the sub-1 view was calculated as the reference hologram. Then, the common object points between sub-1 view and sub-2 view were identified by comparing intensity and coordinate value.

$$\Delta O_{n-1,n} = O_{n-1}(x'_j,y'_j,z'_j) - O_n(x'_j,y'_j,z'_j), \tag{4}$$

where $\Delta O_{n-1,n}$ is the intensity difference between two object points with the same coordinate value. Considering the levels of intensity quantification, any two object points with the intensity difference $|O_{n-1,n}| \le \varepsilon$ (where $\varepsilon \ge 0$) were treated as common object points, where ε is defined as the gray level threshold.

Because the holograms of the common object points were the same, only residual object points should be calculated and added to the reference hologram to generate the hologram of sub-2 view. This action could be extended from sub-$(n-1)$ view to sub-n view. The relationship between the hologram of sub-n view and the hologram of sub-$(n-1)$ view is written in (5).

$$H_{\text{sub}(n)} = H_{\text{sub}(n-1)} + H_{\text{residue[sub}(n-1),\text{sub}(n)]}, \tag{5}$$

where $H_{\text{residue[sub}(n-1),\text{sub}(n)]}$ includes two parts. When $0 < \Delta O_{n-1,n} \le \varepsilon$, the object points only existed in the previous sub-$(n-1)$ view but not in sub-(n) view which should be removed from the reference hologram. When $-\varepsilon \le \Delta O_{n-1,n} < 0$, it indicated the residue object points of sub-(n) view excluding the common object points, which should be added into reference hologram.

Consequently, most computational loads for calculating a sub-hologram were performed from the calculation of the common object points and directly copied from the calculated previous sub-hologram. Therefore, the total computational load was reduced. The final computational load was reduced to:

$$L = \frac{N_{\text{residue[sub}(n-1),\text{sub}(n)]}}{N}, \tag{6}$$

$N_{\text{residual[sub-}(n-1),\text{sub-}(n)]}$ is the sum of the residue object points in adjacent pair of views, excluding their common object points; N is the total number of object points in sub-view.

It was noted that using (4) to identify the common object points directly might cause the intensity quantification error, which increased with the number of views. To reduce the intensity quantification error, the intensity of objects was quantified by the given threshold before the common object point identification, while the quantification error was limited at the range of quantification threshold.

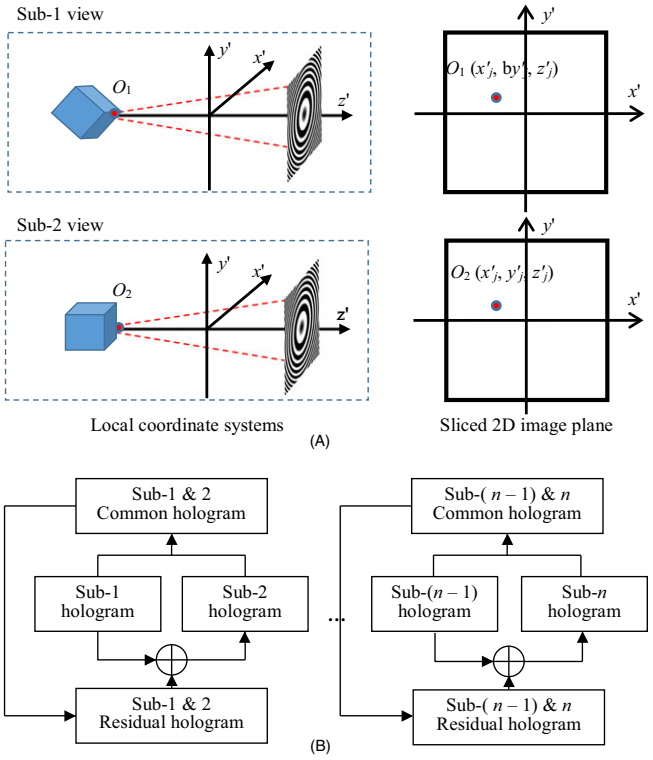

FIGURE 2 (A) Common object points on a pair of adjacent views and (B) flowchart of a proposed method for calculating the hologram

2.2 | Analysis between the common object points and the number of depth layers and angular samplings

It is obvious that the common object points were decreased by their sudden changes in depth for adjacent views. If the changes of depth were not identified by human eyes, they were regarded as located at the same depth. This approximation would reduce the resolution of accommodation cue. Fortunately, accommodation cue is a weak cue for the perception of depth when compared to other cues; moreover, human eyes have quite a low resolution in the depth dimension. Therefore, we could apply merely a few layers to reconstruct the 3D image while still maintaining the necessary depth information to satisfy the continuous accommodation cue [12,13]. Assuming the accommodation cue range is approximately 4D, which is the value for people with an average age of 40 [14], only 28 layers were required from a near point at 25 cm to a far point at

infinity to meet the requirement of human accommodation cue resolution, as shown in Figure 3 [15].

Assuming 3D objects consist of several depth layers, the process of finding common object points were simplified to compare the horizontal and vertical distribution of object points on each depth layer, as measured on an adjacent pair of views. This simplification reduced the common object points searching dimension. Thus, we defined the areas on which object points have the same distribution as the overlapping areas. Note that the common object points were those points located on the overlapping areas which have the same intensity. Therefore, when the overlapping area was larger, more number of common object points were expected to be found.

The sizes of the overlapping areas were different for different depth layers, which depended on the contents and the occlusion relationship. For a better explanation, we used τ to denote different situations that could be divided into two cases: τ is equal to zero or τ is larger than zero. When $\tau = 0$, the object points on the depth layer-n were totally occluded by the object points on the previous depth layer near the viewing point. Therefore, projected image to that viewing point from layer-n was zero and has no common object points between it and its adjacent viewing point. Therefore, we only considered the case of $\tau > 0$, where every depth layer had projected images to the viewing point, as shown in Figure 4.

The red solid lines denote any two adjacent depth layers in viewing point-1. After viewing point-1 was rotated around the point O, which is set as the center of 3D objects, to its adjacent viewing point-2, the 3D objects should be resampled to make each depth layer perpendicular to the viewing axis which was the line that passed through the point O and viewing point P. For convenience, we assumed the viewing point only moved horizontally, so the change in projected image was only related to width while the height was assumed to be the same. The resampled depth layers at viewing point-2 are denoted by red dashed lines. The distance Δl between each depth layer in viewing point-2 was kept the same as in viewing point-1. l is the distance from the depth layer-$(n-1)$ to the point O. The projected image size of depth layer-n to viewing point-1 is τ and the projected image position is $(w, w+\tau)$ on the viewing plane. w is the distance between projected image and viewing axis.

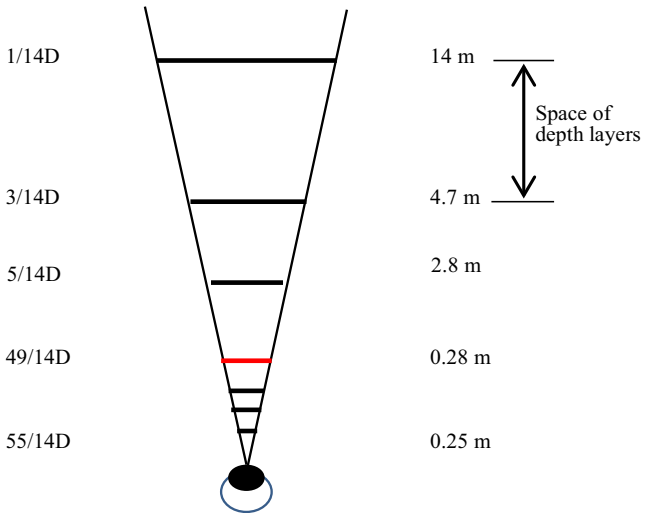

FIGURE 3 Range of accommodation [15]

After viewing point was moved to viewpoint-2, the projected image size of depth layer-n was changed to be:

$$\tau' = d + \delta, \tag{7}$$

where $d = \Delta l \times \sin(\theta)$ is the newly appeared image area that was occluded in viewing point-1; moreover, $\delta = \tau \times \cos(\theta)$. The projected image position was changed to $(w', w'+\tau')$. The overlapping area was obtained by comparing the projected image areas $(w, w+\tau)$ and $(w', w'+\tau')$. The maximum overlapping area was min (τ,τ') for certain special cases, where min is the function returning the smallest value from a supplied set of numeric values.

In most situations, the overlapping areas were calculated by:

$$\text{overlapping area} = \tau\cos(\theta) - D, \tag{8}$$

where D describes the image displacement difference caused by change in viewing point, as calculated by the following equation:

$$D = w - w\cos(\theta) - \Delta l\sin(\theta) \pm l\sin(\theta), \tag{9}$$

where $+$ and $-$ denote the depth layers-$(n-1)$ that was located beyond the point O and between the viewing point and point O, respectively. Equation (9) shows that for those depth layers beyond the point O, the image displacement difference ε may be larger than zero. Therefore, the overlapping area of depth layer-n is smaller than $\tau\cos(\theta)$.

To enlarge the overlapping area, one method was to reduce the angular sampling distance θ. Another method was to reduce the min(τ,τ') by increasing the distance Δl between the depth layers, which implied reducing depth layers of 3D objects. For those depth layers between the point O and the viewing point, when the image displacement difference ε was smaller than zero, the overlapping area of depth layer-n was larger than $\tau\cos(\theta)$. By reducing the angular sampling distance and the depth layers, the maximum overlapping area could reach to the value of min (τ,τ'). Otherwise, reducing the number of depth layers could increase the size of the projected image of each depth layer, which would lead to larger overlapping areas. From the above analysis, it was observed that reducing the angular sampling distance and sampling points in depth dimension could enlarge the overlapping area.

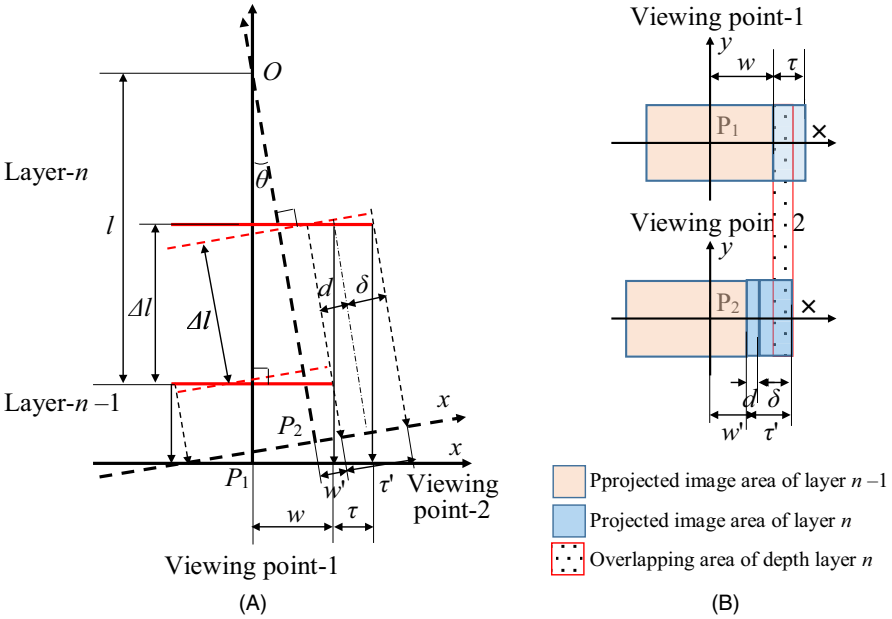

FIGURE 4 (A) Projected image area of different depth layers in adjacent pairs of viewing points; (B) projected image overlapping area

3 | IMPLEMENTATION RESULTS AND DISCUSSION

To demonstrate the results of the proposed algorithm, we performed a numerical simulation and an optical experiment. We chose a car of size 10 mm (width) × 10 mm (height) × 30 mm (depth) as the targeted 3D object. The distance between the object and the hologram was 800 mm. Our program was run by a personal computer (CPU of 2.59 GHz, 8 GB RAM, and 64-bit Operating System) under the MATLAB 2010 environment. The hologram was numerically generated and loaded on the phase-only spatial light modulator (HoloEye, PLUTO) with a resolution of 1,920 × 1,080 and the pixel size of 8 μm. The wavelength of the light source uses was 633 nm.

The 3D object containing 10 depth layers and a hologram divided into 5 × 5 parts were used as an example to prove our proposed method. The 3D object points after hidden parts removal were extracted by occlusion culling method [11] for each sub-hologram. The common and residual object points were found by comparing the pattern and intensity values of each object point for every two adjacent views, as shown in Figure 5. In particular, we adopted the boustrophedon order, and only sub-(n) and sub-(n + 1) were adjacent views, rather than the absolute adjacent location. For example, sub-4 and sub-7 are located adjacent vertically, but we do not treat them as adjacent in the calculation.

The gray level with 256 values is often used to depict the digital images in part because most of today's display and image capture hardware can only support 8-bit images. Consequently, two extreme cases were considered in this paper.

One assumed that all the object points have the same intensity (two gray levels), the other assumed 256 gray levels on object points. In the case of uniform intensity, Figure 5B shows the common and residual areas of sub-1 and sub-2 views. The number of total/common object points was 5,865/5,181. For these common object points, their holograms were the same and calculated only once. Equation (5) is used to calculate the sub-2 hologram, where the actual computed points including $H_{\text{residue}(n)}$ were $H_{\text{residue}(n-1)}$ are 684. Therefore, the computational load was reduced to 11.66%, and the CGH calculated time of sub-2 hologram was reduced from 20.9744 to 2.9862 s. After all the sub-holograms were calculated, they were combined to create the final hologram. To reduce the speckle noise, the multiple random phase method [17,18] was used. The simulation and experiment results reconstructed by 20 holograms with different initial random phases are shown in Figure 6.

In the case of gray level (256 levels), the number of total/common object points was 7,543/2,408. For calculating sub-2 hologram, the actual computed points were 5,135. The computed load was reduced to 68.08%, and the CGH calculated time of sub-2 hologram was reduced from 25.618 to 17.941 s. The results demonstrated that our proposed method was more efficient for the 3D object with slow change in intensity. Fortunately, the intensity changes gradually for most 3D scenes because the surface of these scenes enable diffusion and the distribution of information to the whole hologram plane uniformly. Therefore, similar parts for adjacent views can be located easily and this indicates angular redundancy.

From Section 2, we understand that the computational load reduction depends on the angular sampling distance and depth sampling number. To better illuminate the feasibility of the proposed method, different 3D objects were used for testing. The relationship between the computational time reduction and the angular pitch for different 3D objects are shown in Figure 7, in which two 3D objects —

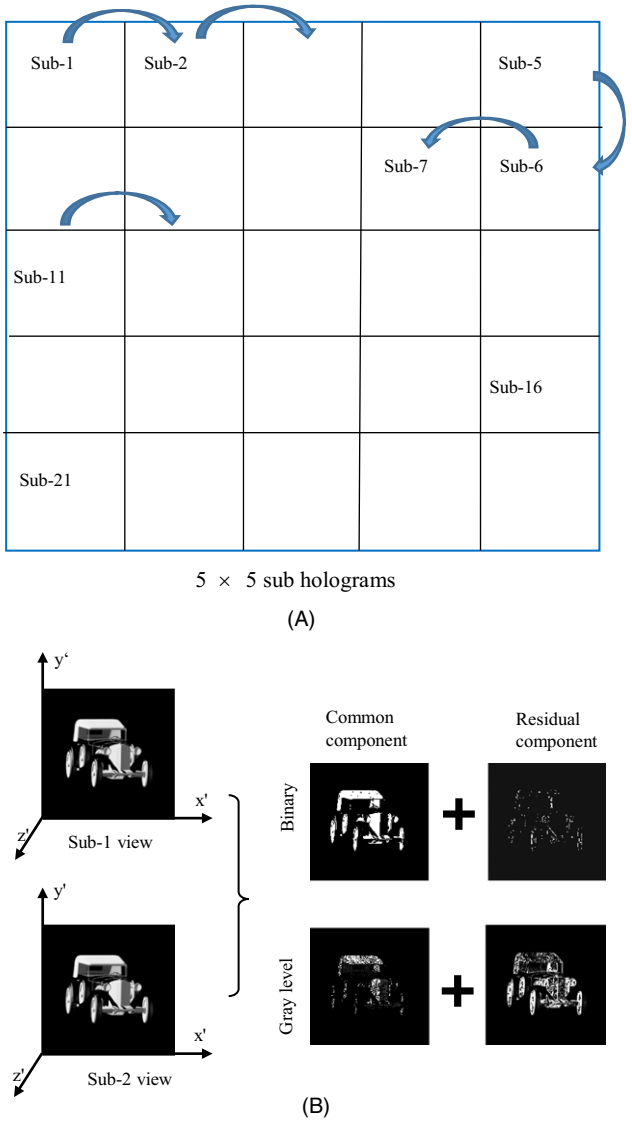

FIGURE 5 (A) Comparing order, (B) Common and residual area of adjacent views. [3D objects are from 3D66 [16], a 3D model open-resource website.]

statue head (14 mm (width) × 18 mm (height) × 10 mm (depth)) and rabbits (20 mm (width) × 20 mm (height) × 100 mm (depth))— are used and their number of layers are 10. It illustrates that as the angular pitch decreases (the more the sub-holograms are used), the adjacent views have more common object points. When the angular pitch is smaller than 0.28° (5 × 5 sub-holograms), the computational time was reduced marginally. Therefore, the proposed method requires only a few angular samplings (sub-holograms) to reduce the computational load, and the results for using 5 × 5 sub-holograms demonstrate that by avoiding recalculation of redundancy, the calculation time for the uniform level intensity is reduced to 5.98%, 6.67%, and 14.22% for the statue head, rabbits, and car, respectively, as shown in Figure 7A. Moreover, the calculation time for the gray level intensity is reduced to 60.98%, 57.9%, and 71.02% for the statue head, rabbits, and car, respectively, as illustrated in Figure 7B.

Conversely, when the angular pitch is fixed, the computational time reduction was determined by the number of depth layers. Normally, the depth map with 256 values was used to describe the distribution of 3D objects in the depth dimension (z-buffer) in computer graphics. In this case, the object points were distributed in 256 depth layers, the number of object points with the same depth value for adjacent views was limited as described in the analysis in section 2.2. Figure 8 shows that the computational time increases when the number of depth layers increases. Note that the calculation time can be more than 100% in this method compared to before the cutting of angular redundancy. Consequently, when the common object points are less than a half of original sub-view area, the calculation load of both $H_{\text{residue}(n)}$ and $H_{\text{residue}(n-1)}$ residual points can be more than 100%. This non-ideal situation can be avoided by applying miniscule angular pitch and limiting the number of layers.

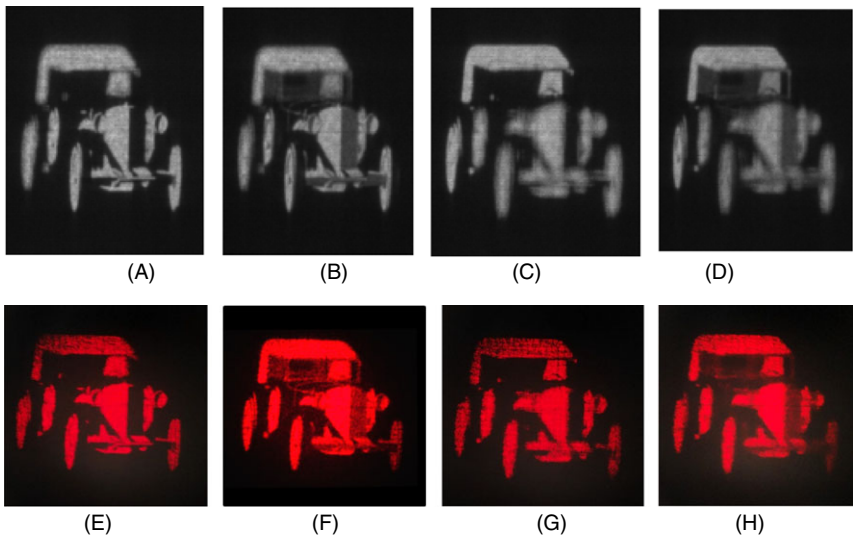

FIGURE 6 Simulation and optical results using proposed method, (A)–(D) the simulation results; (E)–(H) the optical results; (A), (B), (E), and (F) focus on front surface; (C), (D), (G), and (H) rear surface of car; (A), (C), (E), and (G) are binary objects; (B), (D), (F), and (H) are gray level objects. [The 3D objects are from 3D66 [16], a 3D model open-resource website.]

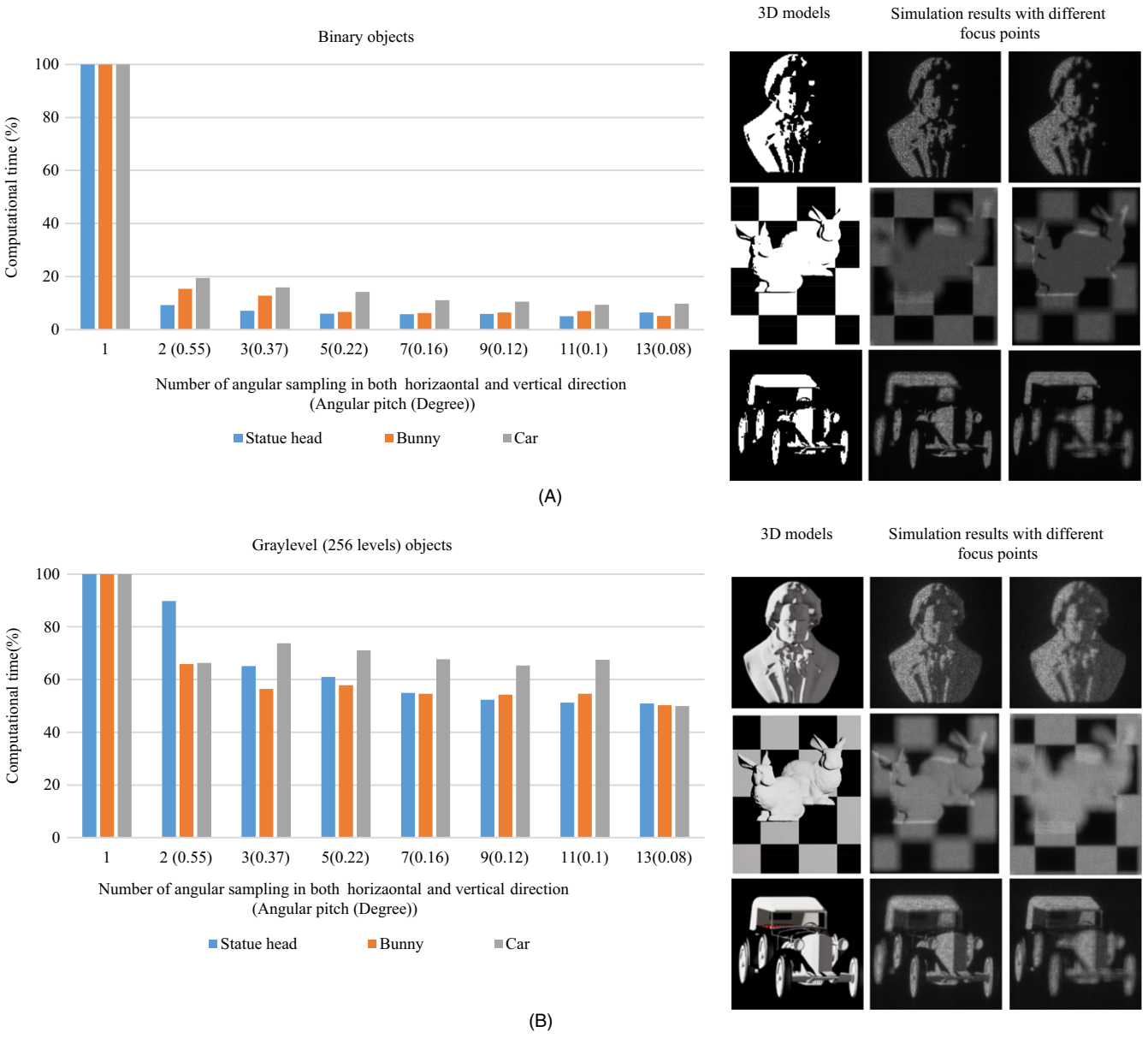

FIGURE 7 Relationship between the computational time and angular sampling distance, (A) Binary objects, (B) Gray level (256 levels) objects. [The 3D objects are from 3D66 [16], a 3D model open-resource website.]

We assume the viewing distance is 250 mm, and the statue head, rabbits, and car have depth size of 12.5 mm, 100 mm, and 30 mm, respectively. Subsequently, the distance to eyes change from 250 mm to 262.5 mm, 350 mm, and 280 mm, respectively. This, can be described by just 2, 10, and 4 layers, respectively, by applying the limitation of human accommodation resolution as illustrated in Figure 4. Therefore, the computational time for uniform intensity can be reduced to 4.73%, 6.67%, and 10.4% for the statue head, rabbits, and car, respectively, as shown in Figure 8A, and for gray level intensity can be reduced to 56.34%, 57.9%, and 66.24% for the statue head, rabbits, and car, respectively, as shown in Figure 8B. The above results were obtained under the fix angular sampling distance of 0.28° (5×5 sub-holograms). The results demonstrated that the computational times were all reduced by cutting angular redundancy for the different shapes of objects. However, for those objects with reflective surfaces, the adjacent views are totally different and may contain very limited angular redundancy; further, the calculation time of the purposed method can be more than 100% when compared to original methods.

Therefore, the proposed method is used to calculate the holograms only for those adjacent views where computational load is considerably less than 100% according to (6), otherwise, the original methods are used. We plan to research and improve the efficiency of the proposed method for 3D objects with different materials in the future.

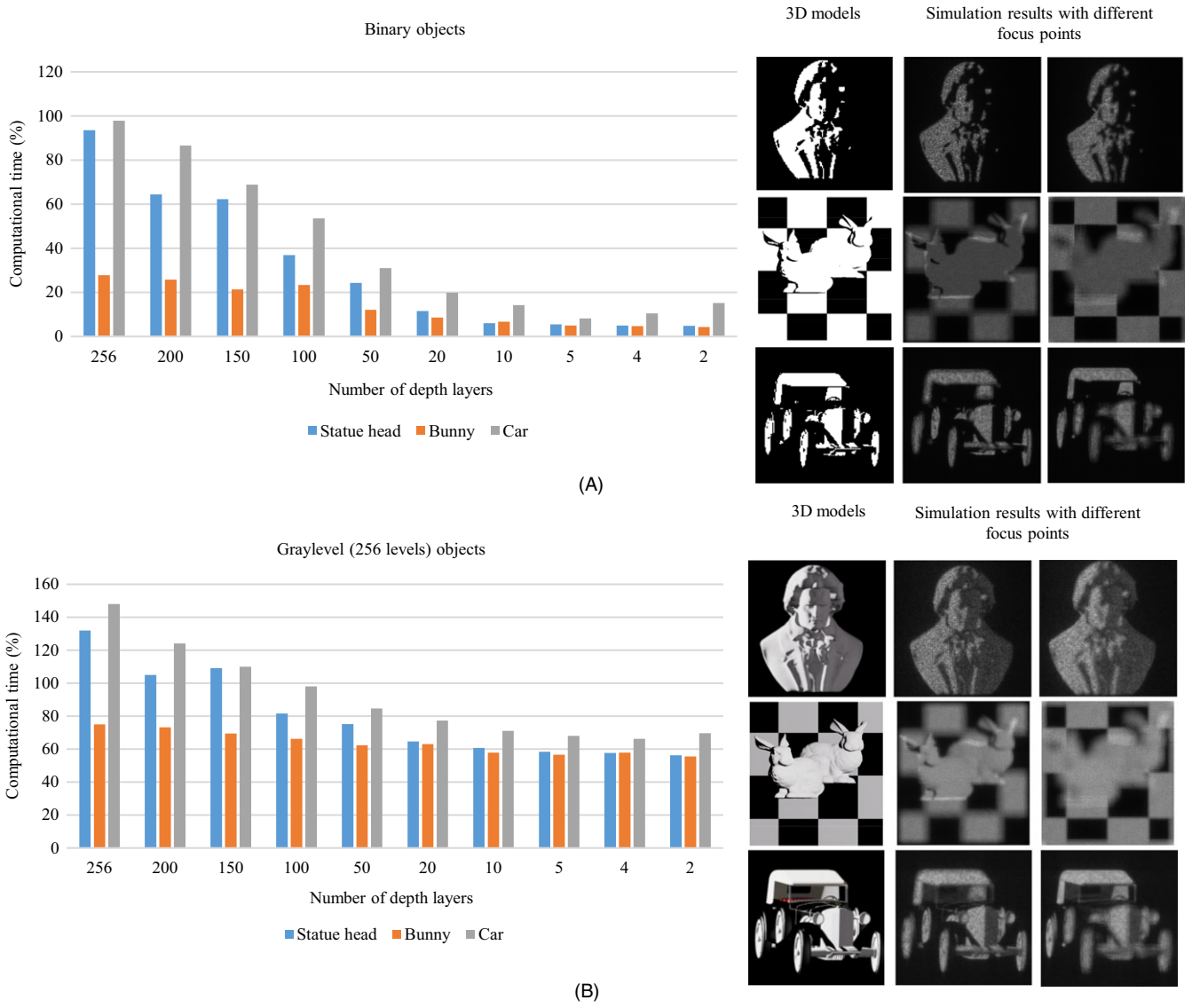

FIGURE 8 Relationship between the computational time and the number of depth layers, (A) Binary objects, (B) Gray level (256 levels) objects. [The 3D objects are from 3D66 [16], a 3D model open-resource website.]

4 | CONCLUSIONS

A hologram calculation method based on angular redundancy cutting was proposed to improve the speed of point-based method hologram computing. In this method, large amounts of object points with the same spatial distribution were found by comparing all the sampling points in each adjacent view, and the holograms of these common object points were only calculated once. This considerably reduced computational loads. Results for different objects demonstrated that the proposed method based on angular redundancy cutting could reduce the calculation time down to 4.73% (statue head), 6.67% (rabbits), and 10.4% (car) for uniform intensity, and 56.34% (statue head), 57.9% (rabbits), and 66.24% (car) for gray level intensity when comparing to the method without cutting redundancy. This method can be applied to 3D objects with any shape but is not suitable for those objects with reflective surfaces. The efficiency of our proposed method for 3D objects with different materials remains to be researched and improved as our future work.

ORCID

Daping Chu https://orcid.org/0000-0001-9989-6238

REFERENCES

1. S. C. Kim, J. H. Yoon, and E. S. Kim, *Fast generation of three-dimensional video holograms by combined use of data compression and lookup table techniques*, Appl. Opt. **47** (2008), 5986–5995.
2. T. Nishitsuji et al., *Simple and fast cosine approximation method for computer-generated hologram calculation*, Opt. Express **23** (2015), 32465–32470.

3. Y. Pan et al., *Fast CGH computation using S-LUT on GPU*, Opt. Express **17** (2009), 18543–18555.
4. Y. Sando, D. Barada, and T. Yatagai, *Fast calculation of computer-generated holograms based on 3-D Fourier spectrum for omnidirectional diffraction from a 3-D voxel-based object*, Opt. Express **20** (2012), 20962–20969.
5. T. Shimobab et al., *Rapid calculation algorithm of Fresnel computer-generated-hologram using look-up table and wavefront-recording plane methods for three-dimensional display*, Opt. Express **18** (2010), 19504–19509.
6. P. Tsang et al., *Holographic video at 40 frames per second for 4-million object points*, Opt. Express **19** (2011), 15205–15211.
7. Z. Zhang et al., *Tunable nonuniform sampling method for fast calculation and intensity modulation in the 3D dynamic holographic display*, Opt. Lett. **38** (2013), 2676–2679.
8. C. Gao et al., *Accurate compressed look-up table method for CGH in 3D holographic display*, Opt. Express **23** (2015), 33194–33204.
9. J. Jia et al., *Reducing the memory usage for effective computer-generated hologram calculation using compressed look-up table in full-color holographic display*, Appl. Opt. **52** (2013), 1404–1412.
10. X.-B. Dong, S.-C. Kim, and E.-S. Kim, *MPEG-based novel look-up table for rapid generation of video holograms of fast-moving three-dimensional objects*, Opt. Express **22** (2014), 8047–8067.
11. J. Jia et al., *Fast and effective occlusion culling for 3D holographic displays by inverse orthographic projection with low angular sampling*, Appl. Opt. **53** (2014), 6287–6293.
12. J. S. Chen, D. Chu, and Q. Smithwick, *Rapid hologram generation utilizing layer-based approach and graphic rendering for realistic three-dimensional image reconstruction by angular tiling*, J. Electron. Imaging **23** (2014), no. 2, 023016:1–023016:7.
13. J. S. Chen, and D. P. Chu, *Improved layer-based method for rapid hologram generation and real-time interactive holographic display applications*, Opt. Express **23** (2015), 18143–18155.
14. J. F. Koretz, C. A. Cook, and P. L. Kaufman, *Accommodation and presbyopia in the human eye. Changes in the anterior segment and crystalline lens with focus*, Investigative Ophthalmology Vis. Sci. **38** (1997), 567–578.
15. S. J. Watt et al., *Achieving near-correct focus cues in a 3D display using multiple image planes*, Proc. Human Vis. Electron. Imaging X, San Jose, CA, USA, 2015, pp. 393–401.
16. 3D66, available at http://www.3d66.com/.
17. M. Makowski et al., *Simple holographic projection in color*, Opt. Express **20** (2012), 25130–25136.
18. T. Shimobaba et al., *Lensless zoomable holographic projection using scaled Fresnel diffraction*, Opt. Express **21** (2013), 25285–25290.

AUTHOR BIOGRAPHIES

Jia Jia received his BEng in mechatronic engineering from the Beijing Institute of Petrochemical Technology in 2003, MEng in mechatronic engineering from the Beijing University of Chemical Technology in 2006, and PhD in optical engineering from the Beijing Institute of Technology in 2013. Subsequently, he became a postdoctoral research fellow at Tsinghua University between 2013 and 2014, a postdoctoral research associate at the Centre for Photonic Devices and Sensors at the University of Cambridge between 2014 and 2017, and a postdoctoral researcher at Microsoft Research Cambridge between 2017 and 2018. His research interests are in the areas of computer holography and 3D displays.

Jhen-Si Chen received his BSc degree in physics from the National Taiwan University in 2009 and his PhD degree in electrical engineering from the University of Cambridge in 2014. He then worked as a postdoctoral research associate at the Centre for Photonic Devices and Sensors at University of Cambridge between 2014 and 2017 before becoming a quantitative researcher. His research interests include holographic displays, algorithms for image hologram calculation, head mounted displays (especially augmented reality), and 3D displays.

Daping Chu received his BSc and MSc degrees in physics from Nanjing University in 1982 and 1986, respectively, and his PhD degree in physics from the University of Warwick in 1994. He worked in the Institute of Physics, Chinese Academy of Sciences, from 1986 to 1991 and the University of Warwick from 1991 to 1998. He moved to Cambridge University in 1998 and joined the Epson Cambridge Laboratory of Epson in 1999 where he was the Executive Researcher until 2007. Subsequently, he returned to Cambridge University and became the Chairman and then Director of the Centre for Advanced Photonics and Electronics and Director of Centre for Photonic Devices and Sensors at the Engineering Department in Cambridge University. His current research interests include space light modulation and phase-only holography for future displays and optical communications, high brightness transreflective displays, laminated electro-active foils for solar shading and smart facade, printable/wearable electronics, high frequency tunable dielectrics for GHz/THz applications, and low cost manufacturing processes.